Cavity enhanced third harmonic generation in graphene

Chris Beckerleg, Tom. J. Constant, Ioannis Zeimpekis, Samuel. M. Hornett, Chris Craig, Daniel W. Hewak and Euan Hendry.

Graphene displays a surprisingly large third order nonlinearity, where conversion efficiencies approaching 10^{-4} *are possible. Moreover, the atomically thin nature of graphene allows for simple integration in cavity designs to increase this even further. Here, we demonstrate an 83-fold enhancement, by comparing resonant and non-resonant wavelengths, in the third harmonic generation from graphene due to the integration of a graphene layer with a resonant cavity. This rather large enhancement occurs as the cavity is resonant both for the fundamental field as well as the third harmonic. We model this effect using the finite difference time domain approach. By comparing our model with experiment, we are able to deduce value of the bulk third order susceptibility of graphene of* $\chi^{(3)} = 4 \times 10^{-17}\,(\mathrm{m/V})^2$.

Graphene is a very promising material for future applications in optoelectronics and photonics [1]. In the visible spectral range, many of the interesting photonic properties of graphene arise due to its linear band structure [2], which infers a wide operation bandwidth in terms of its linear and nonlinear optical properties [3]. At infra-red frequencies, meanwhile, surface plasmons have been experimentally demonstrated [4][5] and their frequency response controlled through the application of an external bias [6]. As a result, graphene is being considered for numerous applications, such as solar-cells and displays, that aim to exploit the combination of a highly conductive yet transparent single layer [7]. Additionally, the broad absorption spectrum of graphene also highlights its potential for photodetection applications [8].

A single layer of graphene is relatively transparent, absorbing only 2.3% of incident visible light [9]. However, this low absorption occurs due the atomically thin nature of graphene, not due to a weak electromagnetic interaction. Moreover, the nonlinear optical interactions with graphene are known to be surprisingly large [10][11][12]. To date there have been several experiments and theoretical investigations into the various nonlinear processes in graphene, from two photon absorption [13] to difference frequency generation [14]. This work focuses on third harmonic generation, which is described with a third order susceptibility $\chi^{(3)}$. Mikhailov predicted that the third order susceptibility of graphene is large, especially in comparison to dielectric materials [15][16]. Meanwhile, third harmonic generation

in graphene has been experimentally investigated in mechanically exfoliated graphene flakes by Kumar et al. [10] and studied theoretically by Zhang et al, with a quantum-dynamical theory [17] and Cheng at al. with a perturbative calculation [18].

Whilst these studies report a comparatively large value of $\chi^{(3)}$ in graphene, the absolute energy conversion is limited by the atomically thin nature of graphene. Therefore, methods for enhancing the nonlinear effects are desirable. One such approach to enhance these nonlinear interactions in graphene is to utilise a planar cavity [19]. To exploit this, Savostianova and Mikhailov have proposed the use of layered structure, consisting of a graphene layer combined with a dielectric on top of a gold film. Their proposed layered structure removes the precise requirements on the frequency and wavevector required for coupling incident photons to surface plasmons, previously demonstrated as a method of enhancing nonlinearity [20]. Such a planar cavity is predicted to enhance the third harmonic generation from graphene by up to two orders of magnitude [19].

In this work, we measure the third harmonic generation from a graphene topped planar cavity, one specifically designed for purpose. We use finite difference time domain (FDTD) numerical modelling to optimise cavity dimensions and thicknesses, as shown in Figure 1a) [21] [22]. We then characterize the integrated cavity in experiment, recording the intensity of generated third harmonic as a function of incident wavelength. By comparing the graphene integrated cavity and the cavity by itself we also demonstrate that the third harmonic signal originating almost entirely from the graphene layer. A clear 83 fold enhancement in the measured third harmonic power is observed at the resonant wavelength, relative to the third harmonic power for non-resonant wavelengths. Finally, by comparing our measurements to our FDTD simulations, we are able to deduce a value of the bulk third order susceptibility of our graphene of $\chi^{(3)} = 4 \times 10^{-17}\,(\mathrm{m/V})^2$.

First, we begin by introducing our FDTD model. We define the linear optical response of our graphene layer through a bulk susceptibility, $\chi^{(1)}$, as;

$$1 + \chi^{(1)} = \epsilon_b + \frac{i\sigma_g}{\epsilon_0 \omega \Lambda}, \tag{1}$$

where ω is the frequency, ϵ_0 the permittivity of free space, $\epsilon_b = 2.5$ the background permittivity [23] and $\Lambda = 0.3\,\mathrm{nm}$, the thickness of the graphene sheet (as determined by ellipsometry measurements [24]). By applying the Kubo formula to graphene, and assuming a temperature $\ll 10^3\,\mathrm{K}$, the surface conductivity of the graphene, σ_g , can be expressed as [25][26][27],

$$\sigma_g = \frac{ie^2 E_f}{\pi\hbar(\omega + i\tau^{-1})} + \frac{e^2}{4\hbar}\left[\theta(\hbar\omega - 2E_f) + \frac{i}{\pi}\log_{10}\left|\frac{\hbar\omega - 2E_f}{\hbar\omega + 2E_f}\right|\right]. \tag{2}$$

This expression accounts for both inter-band and intra-band transitions in the graphene layer. The scattering rate, τ , is defined as, $\tau = E_f \mu / e v_f^2$, and θ is the Heaviside step function. The Fermi energy, $E_f = 0.2$eV, and mobility, $\mu = 1000\,\mathrm{cm}^2$, are set to values typical values for chemical vapor deposition (CVD) graphene [5][28]. Our cavity is formed from a dielectric layer of SiO_2, thickness = 310 nm , and a conducting layer of gold, thickness = 150 nm, as depicted in Figure 1a); the optical responses of these materials are wavelength dependent, as described by Palik [29]. In our experimental sample, a thin (8 nm) layer of titanium is required for adhesion, and this layer is also included in our model for completeness. The entire structure is modelled in 2D, assuming periodic boundary conditions in the planar directions. A vacuum box of 8 μm perpendicular to the graphene by 200 nm in the plane of the graphene is included on the incident half space. Note that, since the gold layer is optically thick, we do not require a vacuum box in the transmission half space. A rectangular, conformal mesh is imposed on the entire structure, with a minimum mesh size of 0.025 nm. The wavelength dependent reflection of the cavity is calculated using a broad band pulse and by integrating the Poynting vector, through a plane, parallel to the graphene layer, 2 μm away from the graphene surface. The nature of the FDTD method allows the fields inside the cavity for different wavelengths to be determined and is shown in Figure 1b) and c).

Nonlinearity is introduced into the model by expanding the polarisation as a power series; introducing an effective third order susceptibility, $\chi^{(3)}$, as; [30]

$$\bar{P} = \epsilon_0(\chi^{(1)}\bar{E} + \chi^{(3)}\bar{E}^3). \tag{3}$$

Here, we treat $\chi^{(3)}$ as a perturbative fit parameter, allowing us to match the generated third harmonic in our model to that observed in experiment. To simulate as close as possible the experimental conditions, a pulse of a fixed carrier frequency, modulated with a gaussian envelope was applied to the graphene layer. This pulse has a full width half maximum (FHWM) of 100 fs, and a peak electric field amplitude of 2.3×10^8 V/m. The central wavelength is varied in the range of 1630 nm to 2400 nm. At each input wavelength, the average power of third harmonic power generated is determined by integrating the Poynting vector across a parallel plane placed in the reflection half space, again 2 μm from the graphene layer. Figure 1d) shows how the generated third harmonic power is predicted to vary with the input wavelength, which is greatly enhanced at the resonance of the cavity. If we define the cavity enhancement as the ratio of the third harmonic power generated by a pulse with the resonant wavelength of 2080nm, to the third harmonic power generated by a pulse with a non-resonant incident wave-

length of 1630nm, we can estimate an enhancement factor of 85. This is comparable to the predication made by Savostianova and Mikhailov [19].

In Figures 1b) and 1c), we plot the time-averaged electric fields calculated for two different cases: on and off resonance. The electric field profile of the resonant incident wavelength, 2080 nm, (blue dotted line) has a maximum at the surface of the graphene layer. The electric field profile of the third harmonic generated by this resonant wavelength, 693 nm (red solid line), also has a maximum at the graphene surface, making the cavity double resonant. Contrasting with the non-resonant case in Figure 1c), plotted for an input wavelength of 1630 nm. While the field for the incident wavelength has a smaller magnitude at the surface of the graphene compared to that for the resonant wavelength, the electric field profile of third harmonic wavelength generated (i.e. 543 nm) is reduced by around a factor of four from the resonant condition.

Taking these modelled parameters as a guide, we fabricated a simple cavity on top of a glass microscope slide, used as a support substrate. A 5nm layer of chrome is thermally evaporated onto the glass to provide an adhesive layer for thermal evaporation of a 150nm layer of gold. The samples are then cleaned in acetone, IPA and water and dried. Before the silicon dioxide deposition, the sample is exposed to an argon etch of 1 minute at a pressure of 30 mTorr and at 30 W RF power to remove possible contaminants. A second 5nm Ti adhesion layer is then sputter-coated at a pressure of 2mTorr and at 300W DC power. Finally, a SiO_2 layer is sputter-coated from a SiO_2 target, with a 2:1 Ar to O_2 gas ratio, at 2 mTorr and at 150W RF power, using an AJA Orion sputterer. Using ellipsometric measurements, the thicknesses of the Ti and SiO_2 layers were confirmed to be 8nm and 309nm, respectively. A 1cm x 1cm area CVD graphene, sourced from graphene-supermarket.com, is then transferred onto the sample using a PMMA assisted transfer technique [31][32].

To measure the third harmonic generation from this layered structure, we designed a two-pulse measurement which allows a background free characterization of the sample, shown in Figure 1a. In this approach, two 100fs laser pulses (1kHz, 1630nm-2400nm central wavelength) incident with angles $\phi = 8°$,$\phi = 30°$, see Figure 1a), are spatially overlapped at the sample interface, spot diameter $\approx 800\,\mu$m. These incident beams were spectrally filtered using a silicon wafer (transmitting for wavelengths $>$ 1130nm) to remove any optical contamination in the beams. The fluence of the pulses is kept below $1\,\mathrm{mJ/cm^2}$, well below the photo-modification threshold for graphene [33]. A thermal power meter, measuring the reflection of the incident pulse, allows for continuous monitoring of the average incident power. The temporal overlap of these two beams at the sample interface is controlled by a variable

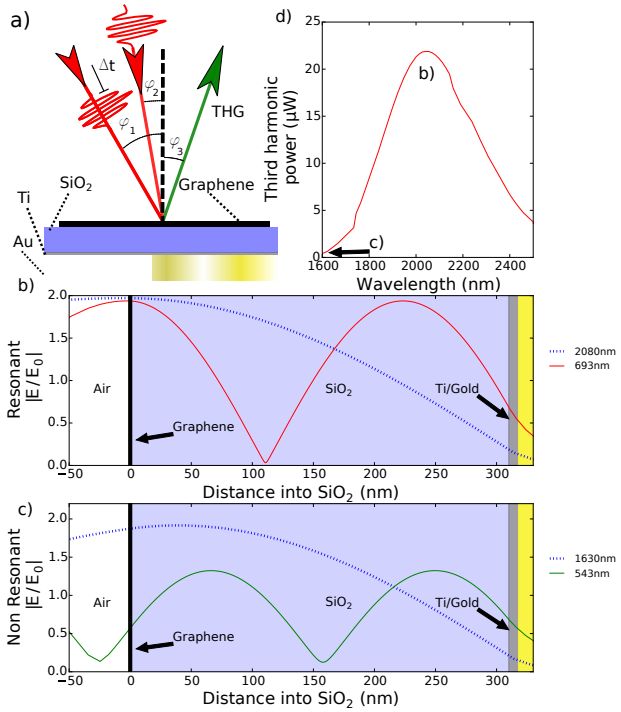

Figure 1: a) Schematic diagram of experimental geometry and sample structure showing the two incident pulses separated by a variable delay time of, Δt, the angles of incidence are; $\phi = 8°$, $\phi = 30°$. The measured third harmonic signal is generated at $\phi = 15°$. The thickness of the layers are; Au 150nm, Ti 8nm, Si02 309nm. b) FDTD modelling of the electric field profile through the stack at the resonance condition. The incident wavelength is 2080nm (blue dotted line) and the third harmonic wavelength is 693nm (red solid line). c) FDTD modelling of the electric field profile through the sample away from the resonance condition. The incident wavelength of 1630nm (solid green line) and a third harmonic wavelength is 543nm (dotted blue). d) FDTD modelling prediction of third harmonic generated as a function of the incident wavelength. The wavelengths of the FDTD electric field profiles in b) and c) are labelled.

time-delay, Δt. When the beams are temporally and spatially overlapped, a third harmonic signal is expected to be generated at four different angles: $8°$, $15°, 23°$and $30°$. To measure the harmonic signal, an avalanche photodiode, protected by an 800nm short pass filter, is placed at $\phi = 15°$, and connected to a lock-in amplifier. One of the incident beams is then modulated at 500 Hz, and the signal from the lock-in amplifier is recorded. The sample is mounted on an xyz micrometer stage so that areas of the sample covered with graphene can be easily compared to areas free from graphene.

Figure 2a) shows a typical measurement of third harmonic power measured as a function of the time delay between pulses for the combined graphene-cavity structure (blue circles). Note that the signal is broader than $\approx 100\,\mathrm{fs}$ due to the non-colinear geometry. The measurement from the cavity alone, red squares on Figure 2a), confirms that the third harmonic signal originates predominantly from the graphene. To further investigate the origin of the signal, the total incident power is varied using a neutral density filter and the resulting third harmonic recorded. The third harmonic power, P_{thg}, is expected to depend on the cube of the incident electric power, P_{inc}. Using a least-squares approach, we find the best fit to our data is $P_{thg} = P_{inc}^{2.98}$ (red line in Figure 2 b). Furthermore, the generated signal is also found to be highly sensitive to the angle of detection, disappearing completely within $\approx$1 degrees of ϕ_3, as expected for a coherent signal such as third harmonic generation.

The effect of the cavity can be investigated by simultaneously varying the wavelengths of both incident pulses from 1630nm to 2400nm and recording the third harmonic power on our detector. We note that the total third harmonic power generated is expected to be approximately four times the measured power, since there are four possible phase matching angles. For this reason, in Figure 2, we plot total harmonic power as approximately four times the measured value. By comparing the measured harmonic signal on (2080nm) and off (1630nm) resonance, we estimate an enhancement factor of 83. This is close to with the value of 85 extracted from FDTD simulations, and with the estimates made by Savostianova and Mikhailov [19]. We note that the width of the resonance recorded in experiment (blue points) is actually narrower than expected from the model (red line). This effect could arise from slightly lower losses in the gold layer, as observed by McPeak et al. [34], or the non-normal angular geometry required in experiment.

To best match the absolute power measured in experiment, we require a bulk susceptibility in our model $\chi^{(3)} = 4 \times 10^{-17}\,(\mathrm{m/V})^2$. This is comparable to the values obtained for the experiments performed by Kumar et al. ($\chi^{(3)} = 4 \times 10^{-17}$,$8 \times 10^{-17}\,(\mathrm{m/V})^2$, [10]) and the theoretical prediction of Zhang et al. ($\chi^{(3)} = 2 \times 10^{-17}\,(\mathrm{m/V})^2$ [17]) but is considerably larger than

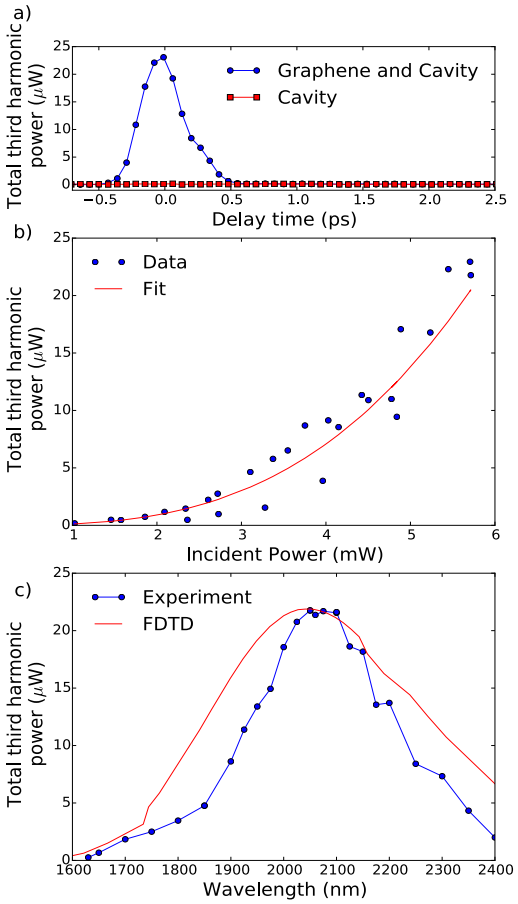

Figure 2: a) A typical time delay measurement of the total third harmonic generated, for $\lambda = 2080\,\text{nm}$, comparing an area on the sample with graphene (blue circles) to the response of just the cavity (red squares). b) Third harmonic generation as a function of the average incident power. The red line is a least-squares fit to the measured data points, found to be $P_{thg} = P_{inc}^{2.98}$. c) The total third harmonic power generated by the cavity, as a function of the incident wavelength, comparing the FDTD modelling results from Figure 1d) (red line) with the measured values (blue circles), for the eye.

the prediction of Chang et al. ($\chi^{(3)} = 6 \times 10^{-19}\,(\text{m/V})^2$)[18]. As noted by Chag et al. themselves, this discrepency may arise from a breakdown of the linear dispersion approximations, non-equilibrium electron dynamics or thermal effects, all of which are not treated in their perturbative model. Note that, with the surprisingly strong cavity effect reported here, we observe a harmonic photon conversion efficiency of 4×10^{-3} for the largest powers used. For essentially a planar structure, such high conversion efficiencies could

be useful in applications where velocity phase matching in bulk crystals is unachievable.

In conclusion, we have shown that graphene displays surprisingly large third order nonlinearity when placed in a planar cavity. We demonstrate an 83-fold enhancement in the third harmonic generation from graphene due to the integration of a graphene layer with a resonant cavity. This rather large enhancement occurs as the cavity is resonant both for the fundamental field as well as the third harmonic field. By modelling this effect using the finite difference time domain approach, we deduce a bulk third order susceptibility of graphene of $\chi^{(3)} = 4 \times 10^{-17}\,(\mathrm{m/V})^2$.

References

[1] K. S. Novoselov, A. K. Geim, S. V. Morozov, D. Jiang, Y. Zhang, S. V. Dubonos, I. V. Grigorieva, and A. A. Firsov, "Electric field effect in atomically thin carbon films.," *Science*, vol. 306, pp. 666–9, oct 2004.

[2] A. K. Geim and K. S. Novoselov, "The rise of graphene.," *Nature materials*, vol. 6, pp. 183–91, mar 2007.

[3] J. M. Dawlaty, S. Shivaraman, J. Strait, P. George, M. Chandrashekhar, F. Rana, M. G. Spencer, D. Veksler, and Y. Chen, "Measurement of the optical absorption spectra of epitaxial graphene from terahertz to visible," *Applied Physics Letters*, vol. 93, no. 13, pp. 3–5, 2008.

[4] E. H. Hwang and S. Das Sarma, "Dielectric function, screening, and plasmons in two-dimensional graphene," *Physical Review B*, vol. 75, p. 205418, may 2007.

[5] L. Ju, B. Geng, J. Horng, C. Girit, M. Martin, Z. Hao, H. A. Bechtel, X. Liang, A. Zettl, Y. R. Shen, and F. Wang, "Graphene plasmonics for tunable terahertz metamaterials.," *Nature Nanotechnology*, vol. 6, pp. 630–4, oct 2011.

[6] Z. Fei, A. S. Rodin, G. O. Andreev, W. Bao, A. S. McLeod, M. Wagner, L. M. Zhang, Z. Zhao, M. Thiemens, G. Dominguez, M. M. Fogler, A. H. Castro Neto, C. N. Lau, F. Keilmann, and D. N. Basov, "Gate-tuning of graphene plasmons revealed by infrared nano-imaging.," *Nature*, vol. 487, p. 82, jul 2012.

[7] F. Bonaccorso, Z. Sun, T. Hasan, and A. C. Ferrari, "Graphene photonics and optoelectronics," *Nature Photonics*, vol. 4, pp. 611–622, aug 2010.

[8] F. Xia, T. Mueller, Y. M. Lin, A. Valdes-Garcia, and P. Avouris, "Ultrafast graphene photodetector," *Nature Nanotechnology*, vol. 4, no. 12, p. 839, 2009.

[9] R. R. Nair, P. Blake, A. N. Grigorenko, K. S. Novoselov, T. J. Booth, T. Stauber, N. M. R. Peres, and A. K. Geim, "Fine structure constant defines visual transparency of graphene.," *Science*, vol. 320, p. 1308, jun 2008.

[10] N. Kumar, J. Kumar, C. Gerstenkorn, R. Wang, H. Y. Chiu, A. L. Smirl, and H. Zhao, "Third harmonic generation in graphene and few-layer graphite films," *Physical Review B*, vol. 87, p. 121406, jan 2013.

[11] E. Hendry, P. J. Hale, J. Moger, A. K. Savchenko, and S. A. Mikhailov, "Coherent nonlinear optical response of graphene," *Physical Review Letters*, vol. 105, no. 9, p. 097401, 2010.

[12] S. A. Mikhailov, "Theory of the nonlinear optical frequency mixing effect in graphene," *Physica E: Low-dimensional Systems and Nanostructures*, vol. 44, pp. 924–927, mar 2012.

[13] Z. Liu, Y. Wang, X. Zhang, Y. Xu, Y. Chen, and J. Tian, "Nonlinear optical properties of graphene oxide in nanosecond and picosecond regimes," *Applied Physics Letters*, vol. 94, no. 2, pp. 1–4, 2009.

[14] T. Gu, N. Petrone, J. F. McMillan, A. V. Zande, M. Yu, G. Q. Q. Lo, D. L. L. Kwong, J. Hone, C. W. Wong, A. van der Zande, M. Yu, G. Q. Q. Lo, D.-L. L. Kwong, J. Hone, and C. W. Wong, "Regenerative oscillation and four-wave mixing in graphene optoelectronics," *Nature Photonics*, vol. 6, no. 8, pp. 554–559, 2012.

[15] R. Hellwarth, "Third Order Optical Susceptibilities of Liquids and Solids.," *Progress in Quantum Electronics*, vol. 5, p. 1, 1977.

[16] S. A. Mikhailov, "Non-linear electromagnetic response of graphene," *Europhysics Letters*, vol. 79, p. 27002, jul 2007.

[17] Z. Zhang and P. L. Voss, "Full-band quantum-dynamical theory of saturation and four-wave mixing in graphene," *Optics Letters*, vol. 36, no. 23, p. 4569, 2011.

[18] J. L. Cheng, N. Vermeulen, and J. E. Sipe, "Third order optical nonlinearity of graphene," *New Journal of Physics*, vol. 18, no. 2, p. 029501, 2016.

[19] N. A. Savostianova and S. A. Mikhailov, "Giant enhancement of the third harmonic in graphene integrated in a layered structure," *Applied Physics Letters*, vol. 107, no. 18, p. 181104, 2015.

[20] T. J. Constant, S. M. Hornett, D. E. Chang, and E. Hendry, "All-optical generation of surface plasmons ingraphene," *Nature Physics*, vol. 12, no. 2, pp. 124–127, 2015.

[21] C. Beckerleg and E. Hendry, "Localized plasmons induced by spatial conductivity modulation in graphene," *Journal of the Optical Society of America B*, vol. 33, no. 10, p. 2051, 2016.

[22] Lumerical Solutions Inc., "Http://www.lumerical.com/tcad-products/fdtd/."

[23] E. Şaşioğlu, H. Hadipour, C. Friedrich, S. Blügel, and I. Mertig, "Strength of effective Coulomb interactions and origin of ferromagnetism in hydrogenated graphene," *Physical Review B*, vol. 95, no. 6, pp. 3–6, 2017.

[24] J. W. Weber, V. E. Calado, and M. C. M. van de Sanden, "Optical constants of graphene measured by spectroscopic ellipsometry," *Applied Physics Letters*, vol. 97, no. 9, p. 091904, 2010.

[25] B. Wunsch, T. Stauber, F. Sols, and F. Guinea, "Dynamical polarization of graphene at finite doping," *New Journal of Physics*, vol. 8, p. 318, dec 2006.

[26] L. A. Falkovsky, "Optical properties of graphene," *Journal of Physics: Conference Series*, vol. 129, p. 5, oct 2008.

[27] T. Stauber, N. M. R. Peres, and A. K. Geim, "The optical conductivity of graphene in the visible region of the spectrum," *Physical. Review. B*, vol. 78, p. 085432, mar 2008.

[28] A. Pirkle, J. Chan, A. Venugopal, D. Hinojos, C. W. Magnuson, S. McDonnell, L. Colombo, E. M. Vogel, R. S. Ruoff, and R. M. Wallace, "The effect of chemical residues on the physical and electrical properties of chemical vapor deposited graphene transferred to SiO2," *Applied Physics Letters*, vol. 99, no. 12, p. 122108, 2011.

[29] E. D. Palik, *Handbook of optical constants of solids.* Academic press, 1998.

[30] Robert Boyd;, *Nonlinear Optics*. Taylor & Francis, 3rd ed., 1992.

[31] X. Li, Y. Zhu, W. Cai, M. Borysiak, B. Han, D. Chen, R. D. Piner, L. Colombo, and R. S. Ruoff, "Transfer of large-area graphene films for high-performance transparent conductive electrodes.," *Nano letters*, vol. 9, p. 4359, dec 2009.

[32] X. Liang, B. A. Sperling, I. Calizo, G. Cheng, C. A. Hacker, Q. Zhang, Y. Obeng, K. Yan, H. Peng, Q. Li, X. Zhu, H. Yuan, A. R. H. Walker, Z. Liu, L. M. Peng, and C. A. Richter, "Toward clean and crackless transfer of graphene.," *ACS nano*, vol. 5, pp. 9144–53, nov 2011.

[33] E. Alexeev, J. Moger, and E. Hendry, "Photo-induced doping and strain in exfoliated graphene," *Applied Physics Letters*, vol. 103, no. 15, p. 151907, 2013.

[34] K. M. McPeak, S. V. Jayanti, S. J. P. Kress, S. Meyer, S. Iotti, A. Rossinelli, and D. J. Norris, "Plasmonic films can easily be better: Rules and recipes," *ACS Photonics*, vol. 2, no. 3, pp. 326–333, 2015.